ARMY RESEARCH LABORATORY

Extracting Stress-Strain and Compressive Yield Stress Information From Spherical Indentation

by Thomas F. Juliano, Mark R. VanLandingham, Tusit Weerasooriya, and Paul Moy

ARL-TR-4229 **September 2007**

NOTICES

Disclaimers

The findings in this report are not to be construed as an official Department of the Army position unless so designated by other authorized documents.

Citation of manufacturer's or trade names does not constitute an official endorsement or approval of the use thereof.

Destroy this report when it is no longer needed. Do not return it to the originator.

Army Research Laboratory
Aberdeen Proving Ground, MD 21005-5069

ARL-TR-4229 **September 2007**

Extracting Stress-Strain and Compressive Yield Stress Information From Spherical Indentation

Thomas F. Juliano, Mark R. VanLandingham,
Tusit Weerasooriya, and Paul Moy
Weapons and Materials Research Directorate, ARL

REPORT DOCUMENTATION PAGE	Form Approved OMB No. 0704-0188

1. REPORT DATE *(DD-MM-YYYY)*	2. REPORT TYPE	3. DATES COVERED (From - To)
September 2007	Final	October 2005–May 2007

4. TITLE AND SUBTITLE
Extracting Stress-Strain and Compressive Yield Stress Information From Spherical Indentation

5a. CONTRACT NUMBER
1120-1120-99

5b. GRANT NUMBER

5c. PROGRAM ELEMENT NUMBER

6. AUTHOR(S)
Thomas F. Juliano, Mark R. VanLandingham, Tusit Weerasooriya, and Paul Moy

5d. PROJECT NUMBER
AH84

5e. TASK NUMBER

5f. WORK UNIT NUMBER

7. PERFORMING ORGANIZATION NAME(S) AND ADDRESS(ES)
U.S. Army Research Laboratory
ATTN: AMSRD-ARL-WM-MA
Aberdeen Proving Ground, MD 21005-5069

8. PERFORMING ORGANIZATION REPORT NUMBER
ARL-TR-4229

9. SPONSORING/MONITORING AGENCY NAME(S) AND ADDRESS(ES)

10. SPONSOR/MONITOR'S ACRONYM(S)

11. SPONSOR/MONITOR'S REPORT NUMBER(S)

12. DISTRIBUTION/AVAILABILITY STATEMENT
Approved for public release; distribution is unlimited.

13. SUPPLEMENTARY NOTES

14. ABSTRACT
In recent years, instrumented indentation has become increasingly used to measure mechanical properties such as elastic modulus and fracture toughness at the micrometer scale. In this work, an experimental method is developed to estimate stress-strain behavior using indentation load-displacement and continuous stiffness measurement data. An attempt is made to subtract plastic behavior out of the loading curve to generate stress-strain data from which elastic modulus and yield stress can be determined. Indentation data generated using three indentation tips with spherical caps (20-, 50-, and 500-μm radii) are compared to bulk mechanical test data for a number of materials important for U.S. Army applications, including polycarbonate, polymethymethacrylate, a tungsten carbide ceramic composite (WC with 11.6% Cobalt), rolled-homogeneous-armor steel, and a titanium alloy (Ti Al6% V4%). The goal of this effort is to be able to predict a macroscopic stress-strain curve from a microscale test using spherical indentation while allowing the indenter to deviate from a perfect spherical shape.

15. SUBJECT TERMS
spherical indentation, stress-strain, rolled-homogenous-armor steel, tungsten carbide, polycarbonate

16. SECURITY CLASSIFICATION OF:			17. LIMITATION OF ABSTRACT	18. NUMBER OF PAGES	19a. NAME OF RESPONSIBLE PERSON
a. REPORT	b. ABSTRACT	c. THIS PAGE			Mark R. VanLandingham
UNCLASSIFIED	UNCLASSIFIED	UNCLASSIFIED	UL	24	19b. TELEPHONE NUMBER (*Include area code*) 410-306-0670

Standard Form 298 (Rev. 8/98)
Prescribed by ANSI Std. Z39.18

Contents

List of Figures iv

List of Tables iv

Acknowledgments v

1. Introduction 1

2. Theory 1

3. Experimental 5

4. Results and Discussion 6

5. Conclusions 11

6. References 12

Distribution List 14

List of Figures

Figure 1. Schematic of indenter contact with a sample surface. (A number of variables from equations 1–5 are depicted.) 2

Figure 2. Curves showing true stress and true strain for compression data (solid lines) and 20-μm-radius indenter data (dotted lines). Curves are shown for (a) Ti-6-4, (b) RHA steel, (c) WC-Co, (d) PMMA, and (e) PC. 9

List of Tables

Table 1. Compressive yield stress values for Ti-6-4, RHA steel, WC-Co, PMMA, and PC measured using compression testing and elastic modulus values measured using ultrasonic testing (Ti-6-4, RHA steel, and WC-Co) and DMA (PMMA and PC)....7

Table 2. Elastic modulus and compressive yield stress values estimated from indentation testing of Ti-6-4, RHA steel, WC-Co, PMMA, and PC using a 20-μm-radius indentation tip. 7

Table 3. Elastic modulus and compressive yield stress values estimated from indentation testing of Ti-6-4, RHA steel, WC-Co, PMMA, and PC using a 50-μm-radius indentation tip. 7

Table 4. Elastic modulus and compressive yield stress values estimated from indentation testing of Ti-6-4, RHA steel, WC-Co, PMMA, and PC using a 500-μm-radius indentation tip. 7

Acknowledgments

This research was supported in part by Thomas F. Juliano’s appointment to the Postgraduate Research Participation Program at the U.S. Army Research Laboratory, administered by the Oak Ridge Institute for Science and Education.

INTENTIONALLY LEFT BLANK.

1. Introduction

Depth-sensing indentation, also referred to as nanoindentation, is a technique in which a hard indenter tool (usually made of diamond or crystalline Al_2O_3) is pressed into a sample surface while load and displacement are measured continuously. It is commonly employed to find elastic modulus and indentation hardness properties of various materials on the microscale (*1–3*). Because indentation crudely resembles a uniaxial compression test, it may seem that stress-strain relationships may be readily discerned from load-displacement data for any tool geometry. However, it has been shown that such a relationship is unique to nonself-similar indenter geometries (i.e., a sphere) but not to pyramidal or conical indenters (*4*).

Pioneering work to determine expressions for indentation stress and strain was done by Tabor and focused primarily on the response of metals to contact loading (*5*). Since that time, a number of studies have attempted to describe indentation stress-strain curves with some promising success (*6–12*). These works have concentrated on a limited modulus range or specific class of material. However, no general study exists that proposes an easily implemented, general framework to estimate the elastic modulus and yield stress of a material for spherical indentation, exclusively using the loading-curve data. Such a procedure is developed in this work, and a number of materials important for military applications are used to exemplify the approach. This work is especially useful in measuring mechanical stress-strain curves on materials that cannot be measured through bulk measurement or materials that are heterogeneous at the microscale. Examples include single material grains, thin films, and microelectromechanical system components.

2. Theory

To derive the relationship for indentation stress and strain, the existing contact mechanics framework is considered. The first analysis of a spherical body orthogonally indenting an elastic halfspace was done by Hertz (*13*). Figure 1 shows a schematic of many variables used in equations 1–5. The elastic displacement of a sphere into a material may be expressed by

$$h_e = \left(\frac{3P}{4E^*}\right)^{2/3}\left(\frac{1}{R}\right)^{1/3}, \tag{1}$$

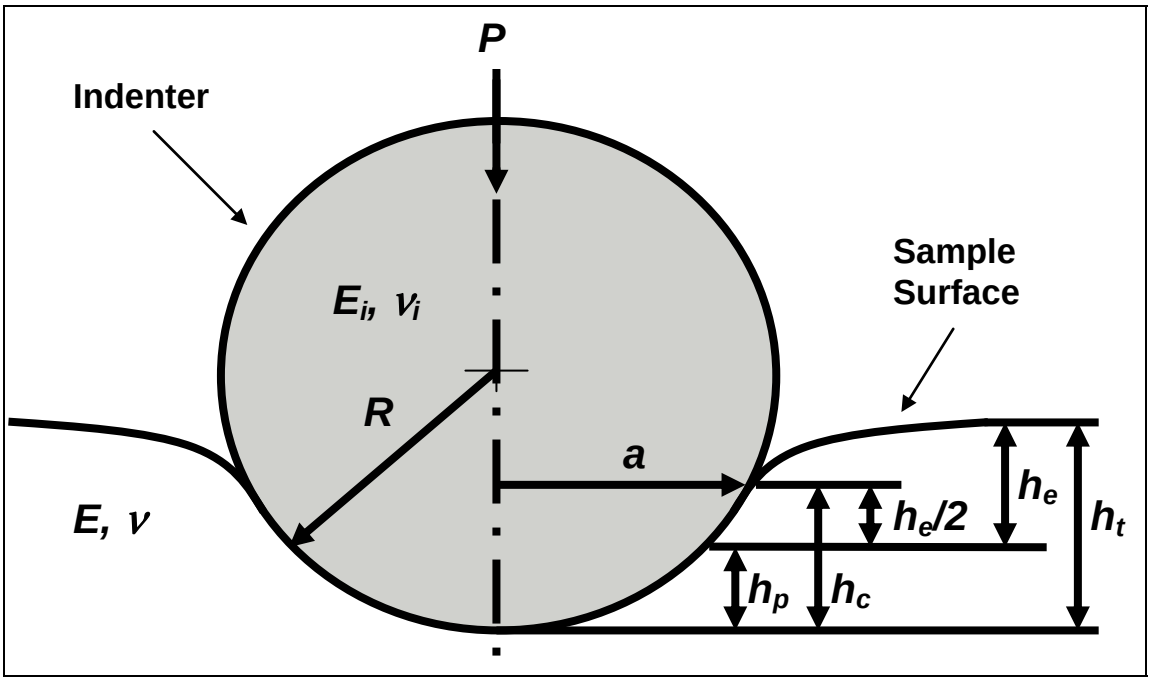

Figure 1. Schematic of indenter contact with a sample surface. (A number of variables from equations 1–5 are depicted.)

where P is the load applied to the indenter, R is the sphere radius, and E^* is the reduced modulus of the material, defined as

$$E^* = \left[\frac{1-\nu^2}{E} + \frac{1-\nu_i^2}{E_i} \right]^{-1} , \tag{2}$$

where ν and E are the Poisson's ratio and elastic modulus of the indented material, respectively, and the subscript i refers to indenter properties (for diamond, E_i is commonly taken as 1141 GPa and ν_i is commonly taken as 0.07).

For purely elastic contact, it has been recognized (*14*) that if the spherical shape is approximated by a paraboloid of revolution, the contact depth can be related to total elastic penetration depth by

$$h_c = \frac{h_e}{2} . \tag{3}$$

As soon as elastic-plastic behavior develops, there exists a plastic depth h_p, in addition to the elastic penetration depth. Therefore, the total penetration depth becomes

$$h_t = h_e + h_p . \tag{4}$$

Because the plastic depth offers no component in the elastic deflection of the material, the total contact depth will be

$$h_c = \frac{h_e}{2} + h_p \ . \tag{5}$$

The contact depth may be determined by the commonly used relation

$$h_c = h_t - \varepsilon \frac{P}{S} \ , \tag{6}$$

where ε is a geometric constant that is 0.75 for a paraboloid of revolution (*14*) and S is the contact stiffness measured continuously throughout the duration of loading by the continuous-stiffness technique (*15*). The continuous stiffness is determined by superimposing a small oscillating excitation force amplitude F_o at a frequency ω on top of the quasistatic applied load and using the relation

$$S = \left[\frac{1}{\frac{F_o}{z_o}\cos\phi - (K_s - M\omega^2)} - \frac{1}{K_f} \right]^{-1} \ , \tag{7}$$

where z_o is the displacement amplitude resulting from F_o, ϕ is the phase angle shift of ω, K_s is the support spring stiffness, M is the mass of the indenter column, and K_f is the frame stiffness. Values for K_s, M, and K_f are determined by the response of a free-hanging indenter tip. The other variables in equation 7 are directly measured continuously during the test, so h_c in equation 6 becomes an experimentally determinable value, since h_t and P are also directly measured.

By combining equations 4 and 5, and substituting in for h_e via equation 1, the relation

$$h_t - h_c = \frac{1}{2}\left(\frac{3P}{4E^*}\right)^{2/3}\left(\frac{1}{R}\right)^{1/3} \tag{8}$$

is obtained, with any displacement due to plasticity inherently accounted for. Note that this equation reduces to equation 1 when displacement is purely elastic. One fact often ignored in indentation analysis is that the radius of spherical and rounded conical indenter tips is often not constant nor is it the quoted nominal value (*16*). Therefore, it is imperative to allow the value of R to vary as a function of depth as it appears in equation 8 to more adequately describe real indenters. It can be shown geometrically that R may be related to the contact depth and projected contact radius a by

$$R = \frac{a^2 + {h_c}^2}{2h_c} \ . \tag{9}$$

For any indenter, a will be a function of h_c, related to the calibrated area coefficients C_n.

$$a = \sqrt{\frac{1}{\pi}\sum_{0}^{n} C_n h_c^{2/2^n}} \quad . \tag{10}$$

Combining equations 2, 8, and 9 and solving for the elastic modulus of the material,

$$E = \frac{1-\nu^2}{\frac{4}{3P}\left[\frac{2(h_t - h_c)}{\left(\frac{2h_c}{a^2 + h_c^{\,2}}\right)^{1/3}}\right]^{3/2} - \frac{1-\nu_i^{\,2}}{E_i}} \quad . \tag{11}$$

By definition, the elastic modulus is the ratio of the true stress over the true strain. As long as true stress can be determined, then an expression for true strain will follow. The definition of true indentation stress is

$$\sigma = \frac{\psi P}{\pi a^2} \quad , \tag{12}$$

or load over projected contact area, where ψ is related to a parameter called the constraint factor (*5*). This factor has been found to be ~0.9 on average when a material is in the purely elastic regime, decreasing to 0.61 when in the elastic-plastic regime, and, finally, tending to 0.35 when full plasticity has been developed (*17*). In the present work, it has been found experimentally that a suitable expression to describe the behavior of ψ through the three loading regimes is

$$\psi = 0.9\left(\frac{h_t}{h_c} - 1\right) \quad . \tag{13}$$

The ratio of h_t/h_c will be equal to 2 if the contact is purely elastic and equal to 1 if the contact is purely plastic. The value of ψ will tend to zero if a purely plastic condition arises, unlike tending to 0.35, as in Francis (*17*). This was done for simplicity and because it more accurately described the results. Because the indentation stress decreases significantly when plastic behavior is the dominating mechanism, equation 13 greatly diminishes in its accuracy when testing extremely plastic materials with a relatively small sphere, e.g., aluminum with a 3-μm nominal radius indenter. When equation 13 is substituted into equation 12, the expression for true indentation stress, which is used throughout this work, is

$$\sigma = \frac{0.9P}{\pi a^2}\left(\frac{h_t}{h_c} - 1\right) \quad . \tag{14}$$

Recognizing that the factor ψ should be linked with P and not projected contact area, the expression for true strain used throughout this work becomes

$$\varepsilon = \left(\frac{0.9P}{\pi a^2 \left(1-\nu^2\right)} \left\{ \frac{h_t}{h_c} - 1 \right\} \right) \left(\frac{4}{2.7P\left(\frac{h_t}{h_c} - 1 \right)} \left[\frac{2\left(h_t - h_c\right)}{\left(\frac{2h_c}{a^2 + {h_c}^2} \right)^{1/3}} \right]^{3/2} - \frac{1-{\nu_i}^2}{E_i} \right) . \qquad (15)$$

All variables in this expression depend only on measurements of load, total displacement into surface, and harmonic contact stiffness.

3. Experimental

Compression and indentation tests were done on cylindrical faces of five different materials with the following dimensions: ~10-mm height and 5-mm diameter, yielding a length-to-diameter ratio of 2:1. The materials used for study were two polymers (polycarbonate [PC] [Lexan 9034 from GE Plastics] and polymethylmethacrylate [PMMA] [Plexiglas G from Atofina Chemicals]), two metal alloys (rolled-homogeneous-armor [RHA] steel [*18*] and a titanium-aluminum6%-vanadium4% [Ti-6-4] alloy), and a ceramic composite made from tungsten carbide and 12%-by-volume cobalt (WC-Co). These materials were chosen because of their range in mechanical properties and widespread use in U.S. Army applications.

Uniaxial compression tests for all materials were performed with true strain controlled compression on an Instron 1331 (MTS Systems). This mode was achieved by using a programmable function generator that sent the command signal feed to the auxiliary input of the Instron machine. Liberal amounts of a lubricant were applied to each specimen to reduce friction between the specimen ends and platens. Also, small grooves were made on the faces of the Ti-6-4 and RHA steel specimens to retain the lubricant to the greatest compression strains possible. No volume change was assumed throughout the end of the tests under pressure. Tests were performed at a strain rate of 0.001 1/s. Compression tests frequently show evidence of nonperfect contact at the beginning of the curve data for most specimens, so only compression-yield-stress values were compared with indentation data. Elastic-modulus values for each material were determined by ultrasonic techniques, as was the case for the Ti-6-4, RHA, and WC-12Co, or by dynamic mechanical analysis (DMA) at 0.1 Hz, as was the case for the PC and PMMA samples.

Indentation tests were run using a Nano Indenter* XP (MTS Systems), which has a load sensing resolution in the μN range and depth sensing resolution in the sub-nm range. Before indentation, all samples were mounted in epoxy and carefully polished to a mirror finish as seen under a 50× microscope objective, using 0.5-μm diamond particle suspensions in the final polishing step. A Dimension 3100 atomic force microscope (Digital Instruments) was used in tapping mode to determine the average root-mean-square roughness value for each sample over a 20- × 20-μm scan area. To eliminate compliance effects due to the epoxy mount, samples were ground from the backside until the sample material was exposed and, finally, were adhered to a stiff aluminum puck. All tests were run at an indentation strain rate (loading rate divided by load) of 0.05 1/s, and the maximum allowed thermal or electronic drift rate was 0.05 nm/s. Different strain rates were attempted but either not enough data points were collected at shallow depths or drift effects would begin to significantly skew the results. Three different indenter tips were used: two diamond sphero-conical geometries with 20- and 50-μm nominal radii and one ruby-spherical geometry with a 500-μm radius. For each geometry and sample, a 4×4 array of indents spaced at least 100 μm apart was generated.

4. Results and Discussion

In table 1, the results from bulk mechanical testing (compression, ultrasonic, and DMA testing) are summarized in terms of compressive yield stress and elastic modulus values. In tables 2–4, estimated compressive yield stress and elastic modulus values are shown for instrumented indentation measurements using 20-, 50-, and 500-μm-radius tips. Compressive yield stress values were determined from compression and indentation testing such that they represent (approximately, in the case of indentation) offset yield stress values at a strain offset of 2%. The compression values shown in table 1 were measured and calculated using standard methods and, thus, are estimates of the actual yield stress values to which the indentation results are compared.

For the two softer materials, PMMA and PC, elastic modulus values determined from indentation for each of the three indentation tips (tables 2–4) were in good agreement with the elastic modulus measured using DMA (table 1). While this agreement is expected of the continuous stiffness measurement (CSM) method, it shows that the indentation stress-strain curves, constructed from the indentation force-displacement data using equations 14 and 15, have the correct slope. For PMMA and PC, modulus values determined using the 20-μm-radius tip were closest, in general, to the DMA measurements. However, for the harder materials (Ti-6-4, RHA steel, and WC-Co), the elastic modulus values from the CSM method and indentation stress-strain slope method were closest to the ultrasonic method (table 1) when using

*Nano Indenter is a registered trademark of MTS Systems Corporation.

Table 1. Compressive yield stress values for Ti-6-4, RHA steel, WC-Co, PMMA, and PC measured using compression testing and elastic modulus values measured using ultrasonic testing (Ti-6-4, RHA steel, and WC-Co) and DMA (PMMA and PC).

Material	Ti-6-4	RHA Steel	WC-Co	PMMA	PC
Compression Yield (GPa)	1.38	1.22	4.51	0.113	0.0682
Bulk Measured Modulus (GPa)	114	205	530	E' = 4.24 E'' = 0.323	E' = 2.21 E'' = 0.029

Table 2. Elastic modulus and compressive yield stress values estimated from indentation testing of Ti-6-4, RHA steel, WC-Co, PMMA, and PC using a 20-μm-radius indentation tip.

Material	Ti-6-4	RHA Steel	WC-Co	PMMA	PC
Compression Yield (GPa)	1.1–1.2	0.9–1.2	5.5–6	0.065–0.075	0.06–0.08
Stress-Strain Curve Modulus (GPa)	65–70	160–180	330–350	2.5–3	1.9–2
CSM Average Modulus (GPa)	97 ± 2	209 ± 2	415 ± 15	4 ± 0.4	2 ± 0.5

Table 3. Elastic modulus and compressive yield stress values estimated from indentation testing of Ti-6-4, RHA steel, WC-Co, PMMA, and PC using a 50-μm-radius indentation tip.

Material	Ti-6-4	RHA Steel	WC-Co	PMMA	PC
Compression Yield (GPa)	0.9–1.3	1–1.1	4.5–5	0.03–0.04	0.05–0.06
Stress-Strain Curve Modulus (GPa)	85–95	180–185	420–440	2.7–2.8	1.8–2.5
CSM Average Modulus (GPa)	110 ± 3	232 ± 5	520 ± 19	3.4 ± 1.3	1.7 ± 0.1

Table 4. Elastic modulus and compressive yield stress values estimated from indentation testing of Ti-6-4, RHA steel, WC-Co, PMMA, and PC using a 500-μm-radius indentation tip.

Material	Ti-6-4	RHA Steel	WC-Co	PMMA	PC
Compression Yield (GPa)	Unmeasurable	Unmeasurable	Unmeasurable	Unmeasurable	Unmeasurable
Stress-Strain Curve Modulus (GPa)	40–50	—	350–400	2.5–2.6	1.3–2
CSM Average Modulus (GPa)	55 ± 3	—	381 ± 60	5.5 ± 0.3	2.2 ± 0.1

the 50-μm-radius tip (table 3). With the exception of the measurements on PC, the greatest deviation in modulus values between indentation and bulk mechanical measurements was observed when using the CSM technique with the 500-μm-radius tip.

Compressive yield stress values for indentation and bulk measurement were in general agreement with one another. For almost all materials, there was less than 33% difference between the two measurement techniques (except for PMMA, where the difference was as much as 73%). The 20- and 50-μm-radius indenters estimated the compressive yield stress effectively. For PMMA and PC, the 20-μm-radius tip gave values closest to the compression tests. For WC-Co, the 50-μm-radius indenter gave the best values. In all cases, the 500-μm-radius indenter was not successful at capturing a compressive yield stress value because of the low overall stress (as described by equation 13) at maximum load. For this reason, it is advised to use spheres with radius values in the range of 10–100 μm in order to reach a suitable stress

state underneath the tool that would make the analysis applicable. A 3-μm-radius tool was used to get compressive yield stress values via this method (data not shown), but results were inconclusive and very scattered. Therefore, it was found that if the stress generated underneath the indenter is too little or too great at shallow depths, this method does not provide good results. This conclusion pertains to soft and hard materials.

Surface roughness played a large role in the accuracy of results. Although all samples were meticulously polished to achieve the smoothest surface possible, roughness values were different between the samples. Average root-mean-square roughness values measured were 2.4 nm for Ti-6-4, 3.9 nm for PC, 7.6 nm for RHA steel, 12.8 nm for WC-Co, and 16.6 nm for PMMA. PMMA, the sample with highest surface roughness, was the most difficult for indentation to describe accurately. For all other samples, measurements with the the 20- or 50-μm-radius tip overlapped compression-test results. When there was high surface roughness for a given sample, it was expected that the modulus and compressive yield stress would be lower than expected. This is because surface asperities create a nonperfect contact between the tip and sample, increasing the contact compliance and lowering modulus and compressive yield stress. In fact, except for the compressive yield stress of WC-Co with the 20-μm sphere, all loading-curve modulus and yield-stress values were lower for indentation compared to compression. This effect was likely attributable to the asperities.

Data showing stress-strain behavior as measured by compression testing with the 20-μm-radius indenter is shown in figures 2a–e. Again, because of imperfect initial loading contact, the compression data was not used to calculate modulus, only compressive yield stress. However, indentation was able to capture both measurements. In all cases, it was seen that the highest indentation stress reached was similar to that of the compression data. Similar curves were generated for the 50-μm-radius indenter. With the 500-μm-radius indenter, curves were also similar except for no clear maximum yield stress in all cases. For all indenters, results were sensitive to where the initial surface contact (h = 0 nm) was taken to be. This point was determined automatically via a defined harmonic contact stiffness value set by the Nano Indenter XP.

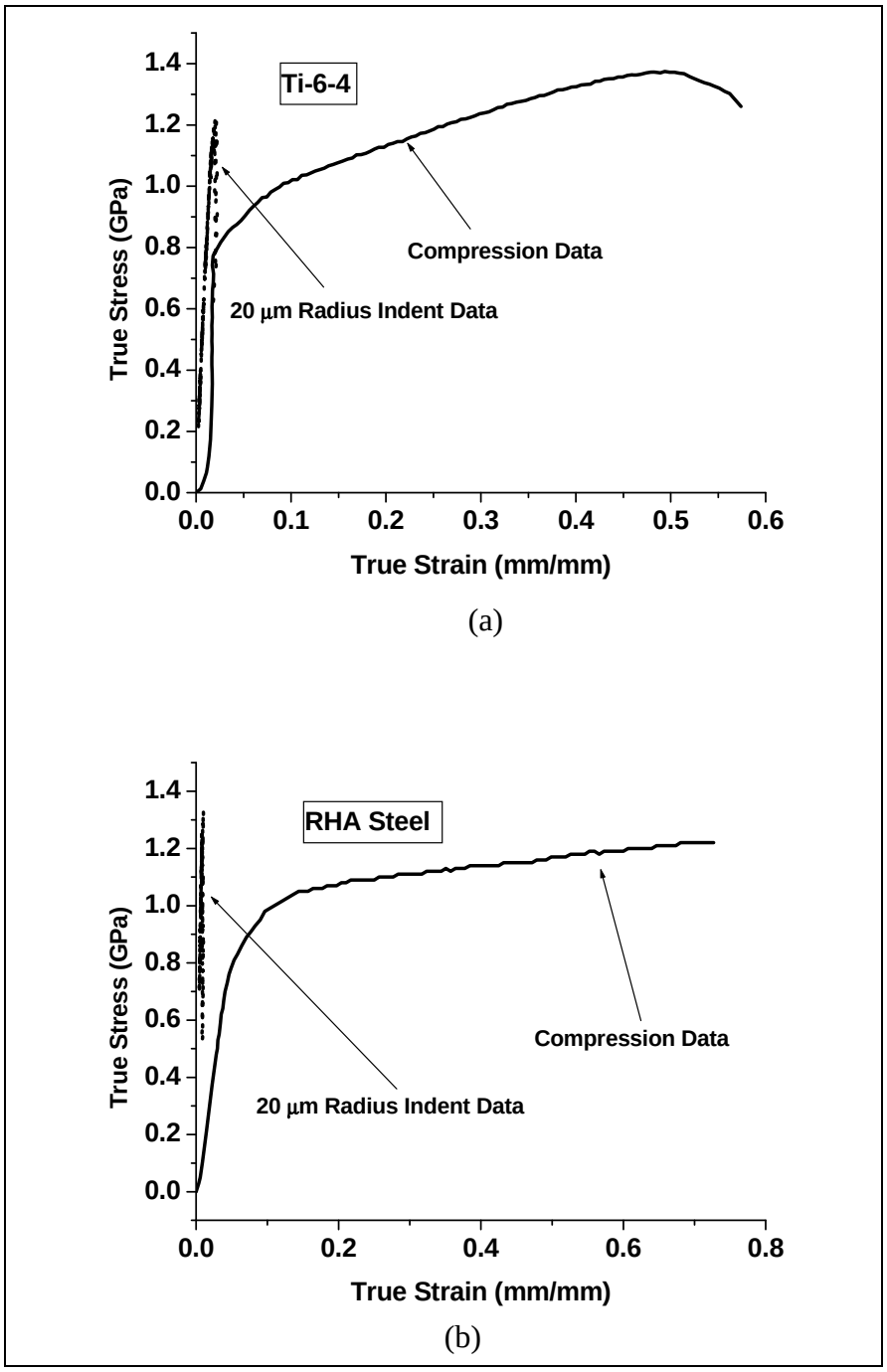

Figure 2. Curves showing true stress and true strain for compression data (solid lines) and 20-μm-radius indenter data (dotted lines). Curves are shown for (a) Ti-6-4, (b) RHA steel, (c) WC-Co, (d) PMMA, and (e) PC.

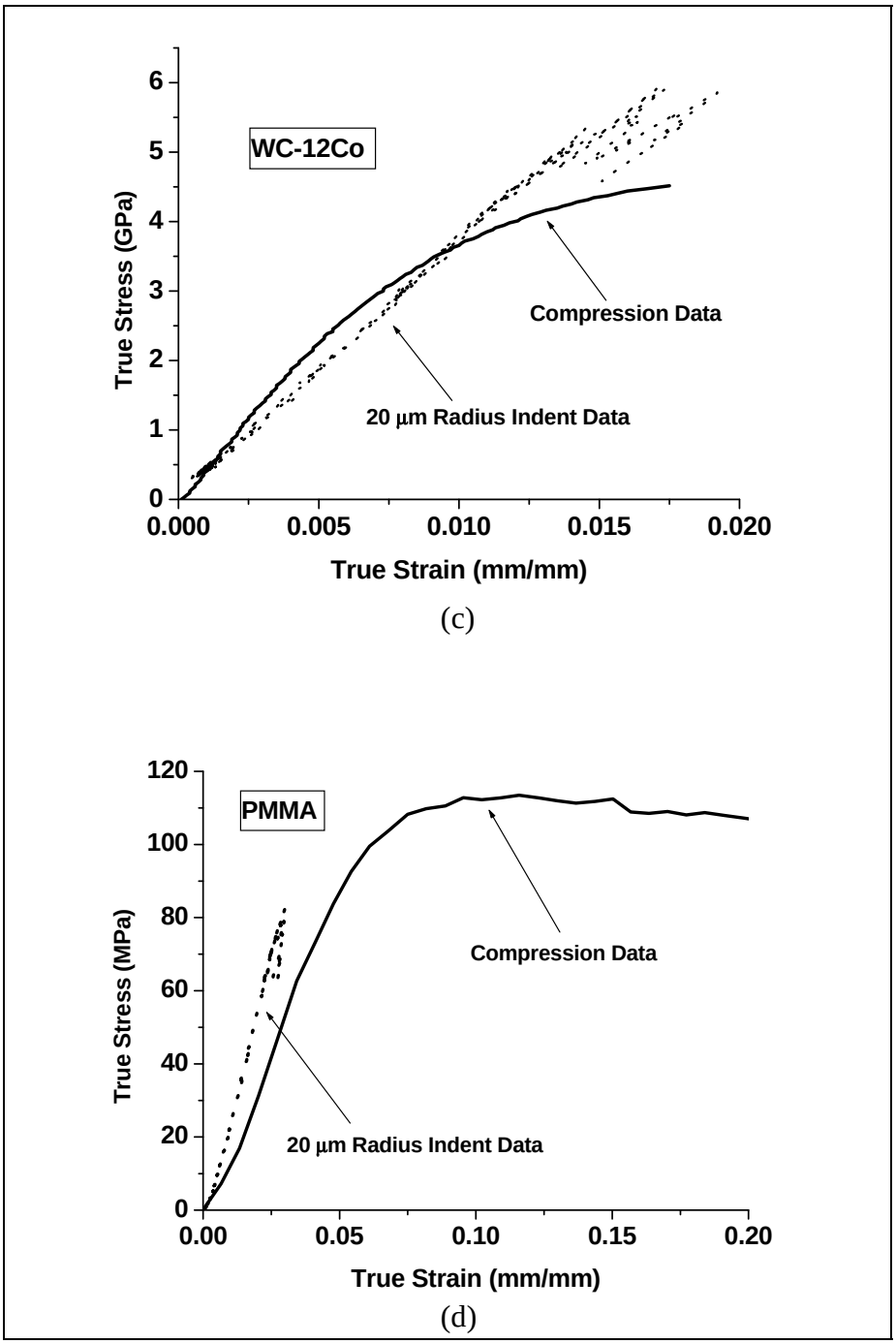

Figure 2. Curves showing true stress and true strain for compression data (solid lines) and 20-μm-radius indenter data (dotted lines). Curves are shown for (a) Ti-6-4, (b) RHA steel, (c) WC-Co, (d) PMMA, and (e) PC (continued).

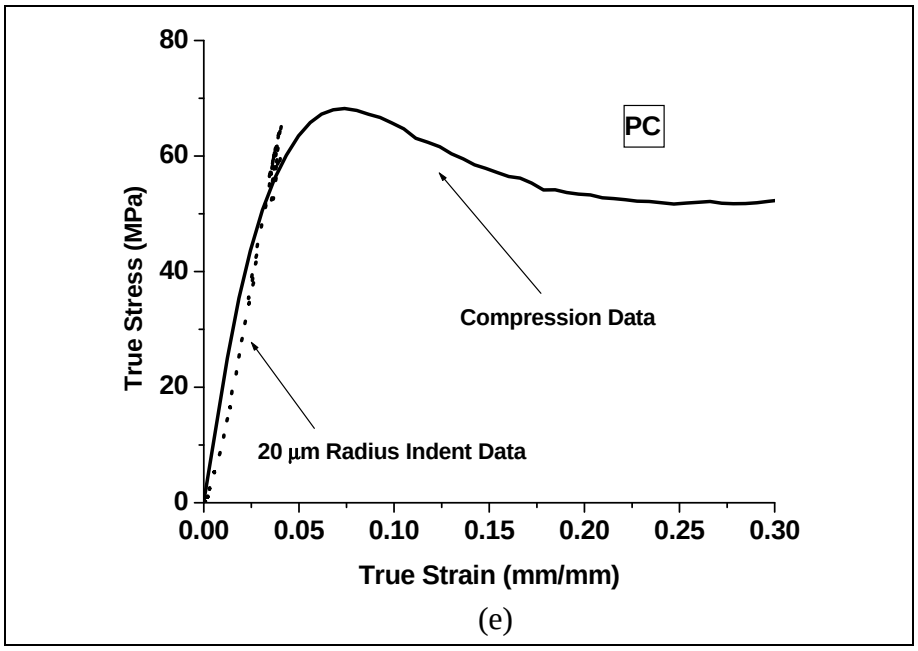

Figure 2. Curves showing true stress and true strain for compression data (solid lines) and 20-μm-radius indenter data (dotted lines). Curves are shown for (a) Ti-6-4, (b) RHA steel, (c) WC-Co, (d) PMMA, and (e) PC (continued).

5. Conclusions

A method was developed that allows stress-strain curves to be determined from load-displacement indentation data. These curves were shown to provide a fair estimation of modulus and compressive yield stress information when compared to bulk values, with typical errors being 33%, at worst, and within just a few percent, at best. Successful measurement was taken for materials with a range of modulus and yield properties. The method developed makes use of analyses by Hertz, Tabor, and Francis, by subtracting out the plastic contribution during the indentation. Factors such as radius of the sphere and surface roughness played a role in the adequacy of the method. For the materials studied, Ti-6-4 and PC had the greatest agreement between macroscale and microscale data. Future work should include exploring a more rigorous framework for determining the constraint factor, determining quantitatively the effect of surface roughness on the method's efficacy, using the approach for small-scale features, and studying the effect of loading rate on results.

6. References

1. Oliver, W. C.; Pharr, G. M. An Improved Technique for Determining Hardness and Elastic Modulus Using Load and Displacement Sensing Indentation Experiments. *J. Mater. Res.* **1992**, *7* (6), 1564–1583.
2. Field, J. S.; Swain, M. V. A Simple Predictive Model for Spherical Indentation. *J. Mater. Res.* **1993**, *8* (2), 297–306.
3. Oliver, W. C.; Pharr, G. M. Measurement of Hardness and Elastic Modulus by Instrumented Indentation: Advances in Understanding and Refinements to Methodology. *J. Mater. Res.* **2004**, *19* (1), 3–20.
4. Cheng, Y. T.; Cheng, C. M. Can Stress-Strain Relationships be Obtained From Indentation Curves Using Conical and Pyramidal Indenters? *J. Mat. Res.* **1999**, *14* (9), 3493–3496.
5. Tabor, D. *Hardness of Metals*. Clarendon Press: Oxford, UK, 1951; p 175.
6. Field, J. S.; Swain, M. Determining the Mechanical Properties of Small Volumes of Material From Submicrometer Spherical Indentations. *J. Mater. Res.* **1995**, *10* (1), 101–112.
7. Fischer-Cripps, A. C.; Lawn, B. R. Indentation Stress-Strain Curves for "Quasi-Ductile" Ceramics. *Acta Materialia* **1996**, *44* (2), 519–527.
8. Taljat, B.; Zacharia, T.; Kosel, F. New Analytical Procedure to Determine Stress-Strain Curve From Spherical Indentation Data. *Int. J. Solids Structures* **1998**, *35* (33), 4411–4426.
9. Iwashita, N.; Swain, M.; Field, J. S.; Ohta, N.; Bitoh, S. Elasto-Plastic Deformation of Glass-Like Carbons Heat-Treated at Different Temperatures. *Carbon* **2001**, *39*, 1525–1532.
10. Herbert, E. G.; Pharr, G. M.; Oliver, W. C.; Lucas, B. N.; Hay, J. L. On the Measurement of Stress-Strain Curves by Spherical Indentation. *Thin Solid Films* **2001**, *398*, 331–335.
11. Hochstetter, G.; Jimenez, A.; Cano, J. P.; Felder, E. An Attempt to Determine the True Stress-Strain Curves of Amorphous Polymers by Nanoindentation. *Tribology International* **2003**, *36* (12), 973–985.
12. Ogasawara, N.; Chiba, N.; Chen, X. Representative Strain of Indentation Analysis. *J. Mat. Res.* **2005**, *20* (8), 2225–2234.
13. Hertz, H. On the Contact of Elastic Solids. *J. Reine Angew. Math.* **1881**, *92*, 156–171.
14. Sneddon, I. N. The Relation Between Load and Penetration in the Axisymmetric Boussinesq Problem for a Punch of Arbitrary Profile. *Int J. Engng Sci.* **1965**, *3*, 47.

15. Oliver, W. C.; Pharr, G. M. An Improved Technique for Determining Hardness and Elastic Modulus Using Load and Displacement Sensing Indentation Experiments. *J. Mater. Res.* **1992**, *7* (6), 1564.

16. VanLandingham, M. R.; Juliano, T. F.; Hagon, M. J. Measuring Tip Shape for Instrumented Indentation Using Atomic Force Microscopy. *Meas. Sci. Technol.* **2005**, *16*, 2173–2185.

17. Francis, H. A. Phenomenological Analysis of Plastic Spherical Indentation. *Journal of Engineering Materials and Technology-Transactions of the Asme* **1976**, *98* (3), 272–281.

18. Weerasooriya, T.; Moy, P. Effect of Strain-Rateon the Deformation Behavior of Rolled-Homogeneous Armor (RHA) Steel at Different Hardnesses. Presented at the 2004 SEM X International Congress and Exposition on Experimental Mechanics, Costa Mesa, CA, 7–10 June 2004.

NO. OF COPIES	ORGANIZATION
1 (PDF ONLY)	DEFENSE TECHNICAL INFORMATION CTR DTIC OCA 8725 JOHN J KINGMAN RD STE 0944 FORT BELVOIR VA 22060-6218
1	US ARMY RSRCH DEV & ENGRG CMD SYSTEMS OF SYSTEMS INTEGRATION AMSRD SS T 6000 6TH ST STE 100 FORT BELVOIR VA 22060-5608
1	DIRECTOR US ARMY RESEARCH LAB IMNE ALC IMS 2800 POWDER MILL RD ADELPHI MD 20783-1197
3	DIRECTOR US ARMY RESEARCH LAB AMSRD ARL CI OK TL 2800 POWDER MILL RD ADELPHI MD 20783-1197

ABERDEEN PROVING GROUND

1	DIR USARL AMSRD ARL CI OK TP (BLDG 4600)

NO. OF COPIES	ORGANIZATION
31	AMSRD ARL WM B
	J MORRIS
	J NEWILL
	M ZOLTOSKI
	AMSRD ARL WM M
	R DOWDING
	S MCKNIGHT
	AMSRD ARL WM MA
	CHIEF
	A BUJANDA
	D O’BRIEN
	L GHIORSE
	R JENSEN
	E WETZEL
	P MOY
	AMSRD ARL WM MB
	CHIEF
	R CARTER
	W DRYSDALE
	R EMERSON
	R KASTE
	M MINNICINO
	J SOUTH
	M STAKER
	J SWAB
	AMSRD ARL WM MC
	CHIEF
	AMSRD ARL WM MD
	E CHIN
	B CHEESEMAN
	G GAZONAS
	AMSRD ARL WM T
	A CARDAMONE
	P BAKER
	AMSRD ARL WM TA
	S SCHOENFELD
	AMSRD ARL WM TD
	CHIEF
	D DANDEKAR
	T WEERASOORIYA

INTENTIONALLY LEFT BLANK.